




Tilting Planets during Planet Scattering

Gongjie Li 

Center for Relativistic Astrophysics, School of Physics, Georgia Institute of Technology, Atlanta, GA 30332, USA; gongjie.li@physics.gatech.edu
Received 2021 March 25; revised 2021 May 25; accepted 2021 May 28; published 2021 June 25

Abstract

Observational constraints on planetary spin axis have recently become possible, and they have revealed a system that favors large spin-axis misalignment, low stellar spin–orbit misalignment, and high eccentricity. To explain the origin of such systems, we propose a mechanism that could tilt the planetary spin axis during planet–planet scattering, which is a natural outcome of in situ formation and disk migration. Specifically, we show that spin–orbit resonances could occur for a short time period during the scattering processes, and excite the misalignment of a planet’s spin axis. This typically leads to planets with large spin misalignment and a wide range of eccentricities and inclinations.

Unified Astronomy Thesaurus concepts: [Exoplanet formation \(492\)](#); [Exoplanet astronomy \(486\)](#); [Exoplanet dynamics \(490\)](#)

1. Introduction

Tilt of the planetary spin axis provides important constraints on the formation and the subsequent dynamical evolution of the planetary systems (Lissauer 1993). For the solar system planets, the tilt of the planets has been well explored, and a large number of factors could influence the obliquity (spin–orbit misalignment) of the planets. For instance, the terrestrial planets have all encountered chaotic obliquity variations in the past due to secular resonances between planetary spin axis and orbital perturbation (Ward 1973; Laskar & Robutel 1993; Touma & Wisdom 1993; Li & Batygin 2014), while the spin axes of Mercury and Venus have been stabilized by tidal dissipation and that of the Earth has been stabilized by the capture of the Moon. For the gas giants, Jupiter’s obliquity remains low, while Saturn has a larger obliquity of 26.7° . Both of them could be affected by resonances with either Uranus or Neptune during planet migration (Ward & Hamilton 2004; Vokrouhlický & Nesvorný 2015). Uranus has a large obliquity above 90° , and this is likely due to giant impacts as well as spin–orbit resonances in the presence of the circumplanetary disk (e.g., Slattery et al. 1992; Morbidelli et al. 2012; Rogoszinski & Hamilton 2020).

Little is known about extrasolar planets, compared to those residing in the solar system. Theoretical estimates of the obliquity variations of planets have been done for those residing in the habitable region, motivated by the fact that obliquity determines the latitudinal distribution of stellar radiation and is important for the snowball transition of planets (e.g., Kane & Torres 2017; Shan & Li 2018; Quarles et al. 2019, 2020; Saillenfest et al. 2019). For instance, it is shown that Kepler 62f and Kepler 186f do not require a massive moon to stabilize their obliquity, in contrast to Earth. In addition, different mechanisms have been proposed to tilt the spin axes of exoplanets during planet formation, such as via planet–disk interactions (Millholland & Batygin 2019; Martin et al. 2020; Su & Lai 2020), planet–planet interactions (Ward & Hamilton 2004; Vokrouhlický & Nesvorný 2015; Quillen et al. 2018; Millholland & Laughlin 2019), planet collisions (Li & Lai 2020) and satellite migration (Saillenfest et al. 2021).

Many observational techniques have been proposed to constrain the obliquities of planets (Barnes & Fortney 2003;

Gaidos & Williams 2004; Carter & Winn 2010; Schwartz et al. 2016). In particular, the first constraint on the orientation of the spin axis of a planet mass companion has been made for the directly imaged system 2MASS J012250932439505 (2M0122), using the projected rotation rates for the companion (Bryan et al. 2020). It was found that while the stellar obliquity prefers alignment, the companion obliquity favors misalignment. In addition, the planet mass companion is most likely in a high eccentricity orbit. It was suggested that, while secular spin–orbit resonances (due to the low planetary spin precession rate), collisions (due to high escape velocity of the massive planet), and Kozai–Lidov oscillations (due to low stellar obliquity) are all unlikely to be causing the tilt of the planetary spin axis, gravitoturbulent disks provide a promising scenario to tilt the planetary spin axis.

To further explore mechanisms that lead to planets with large obliquities, low stellar obliquities, and high eccentricities, which are currently out of spin–orbit resonances, we investigated spin-axis variations during planet–planet scattering. Planet–planet scattering naturally leads to orbits with a wide range of eccentricities and inclinations. In addition, planet–planet scattering is a common outcome of planet formation, as planets form in a nearly maximally packed configuration in the protoplanetary disk (Kokubo & Ida 2002; Goldreich et al. 2004; Ida & Lin 2004). Once the disk dissipates, mutual planetary perturbations will lead to eccentricity and inclination growth, as well as close encounters between the planets (e.g., Chambers et al. 1996; Rasio & Ford 1996; Lin & Ida 1997; Adams & Laughlin 2003; Chatterjee et al. 2008; Ford & Rasio 2008; Petrovich et al. 2014). It has been found that planetary scattering could lead to high eccentricity planets and planets with large stellar spin–orbit misalignment. More recently, it was responsible for the formation of many of the warm jupiters (Mustill et al. 2017; Freikh et al. 2019; Anderson et al. 2020).

During planet–planet scattering, planets may collide with each other, and the spin axis of the merger product could be misaligned due to the conservation of angular momentum and linear momentum (Li & Lai 2020). However, the changes in eccentricities and inclinations typically remain low during collisions. Thus, in our paper, we focused on scattering of planets with no collisions. The fraction of systems that avoid

collisions increases with increasing planetary semimajor axis and planetary masses.

It is often assumed that the spin axis experiences little change during scattering, since the sizes of the planets are small, and the total torque on the planets during the scattering encounter are too negligible to tilt the planet (Lee et al. 2007). Nevertheless, here we show that spin–orbit resonances could take place during the scattering events and tilt the planetary spin axis. This could lead to misaligned planets with a wide range of eccentricities and inclinations, as well as lower spin rate compared to that due to collisions. This effect is similar to the tilt of the solar system giant planets during planet migration.

The paper is organized as follows: we describe our scattering experiments in Section 2, where Section 2.1 presents the setup of the scattering experiments, Section 2.2 focuses on one illustrated example, and Section 2.3 summarizes the results of the Monte Carlo simulations of the scattering experiments. Then, we explore a larger parameter space and describe the dependence of planetary spin axis inclination on the properties of the planet system in Section 3. In the end, we summarize the main findings in Section 4.

2. Scattering Experiments

2.1. Experiment Setup

We run N -rigid-body simulations to study the spin-axis evolution during planet–planet scattering, using the GRIT simulation package (Chen et al. 2021). The GRIT simulation package contains a symplectic Lie-group integrator that we developed to simulate systems with gravitationally interacting rigid bodies (Chen et al. 2021). Different from the integrator developed by Touma & Wisdom (1994), we do not assume the orbits to be near Keplerian, and thus, this integrator is suitable to study the effects during planet–planet scattering. Tidal dissipation is included in the GRIT simulation package. However, we note that tides make negligible effects in the final distribution of planetary obliquity, and thus we do not include tide for our scattering experiments. General relativistic effects (first-order post-Newtonian) are included in the scattering experiments since planets can be scattered very close to the host star.

In our default set of simulations (results summarized in Section 2.3), we include three planets in each of the planet systems. We set the initial eccentricities of the planets to range between 0 and 0.1 distributed uniformly and the initial inclination to range between 0° and 2° uniformly. Higher initial eccentricities allow instabilities to occur faster. We vary the initial orbital parameters (e.g., changing the initial eccentricities to range between 0 and 0.05 in Section 3). We set the planets to be separated by $3.5R_{\text{H,mutual}}$ from each other, where the mutual Hill radius is expressed as follows:

$$R_{\text{H,mutual}} = \left(\frac{m_1 + m_2}{3M_{\text{star}}} \right)^{1/3} \frac{a_1 + a_2}{2}, \quad (1)$$

where m_1 and m_2 and a_1 and a_2 are the masses and semimajor axes of the two planets separately, and we placed the innermost planet at 1 au. The argument of pericenter, longitude of ascending node and mean anomaly of the planets are uniformly distributed between 0 and 2π .

For each of the planets, we set their masses to range between $1m_{\text{jup}}$ and $2m_{\text{jup}}$ distributed uniformly. The mass range is set

arbitrarily, and we discuss the effects with different planet masses in Section 3. We set the radius of the planets to be one Jupiter radius, and the spin rate of the planets to be 30% of the breakup spin rate. The oblateness of the planets is obtained using the Darwin–Radau relation (Murray & Dermott 2000):

$$\mathbb{C} \equiv \frac{C}{m_p R_p^2} = \frac{2}{3} \left[1 - \frac{2}{5} \left(\frac{5q}{2f} - 1 \right)^{1/2} \right], \quad (2)$$

where C is the planet’s moment of inertia around the rotational axis, m_p is the mass of the planet, R_p is the radius of the planet, q represents the relative importance of the centripetal acceleration and f represents oblateness. We assume the moment of inertia coefficient $\mathbb{C} = 0.26$ for gas giants and obtain $f = 0.067$. This is similar to the oblateness of Jupiter ($f_{\text{jup}} = 0.06487$), and smaller than that of Saturn ($f_{\text{sat}} = 0.09796$). We assume the love number of the gas giants to be $k_2 = 0.5$, following the $n = 1$ polytrope density distribution. We assume the stellar J_2 moment to be 2×10^{-7} , similar to the Sun, though we note that the stellar J_2 moment has little effect on the final distribution of the planetary spin axes.

We run the simulations for 1 Myr (10^6 times the innermost planet’s period). This is much longer than the instability time of the planets with a separation of $3.5R_{\text{H,mutual}}$ (~ 300 yr) (Chatterjee et al. 2008). The time step is set to be 10^{-4} yr, less than 5% of the spin period of the planets.

2.2. Illustrative Example

To illustrate how the planetary spin axes are tilted during planet scattering, we include here an illustrative example using one of the Monte Carlo draws. The masses of the planets are $1.1643m_{\text{jup}}$, $1.0090m_{\text{jup}}$, and $1.6349m_{\text{jup}}$ separately, and the initial eccentricities and inclinations are 0.052255, 0.098151, and 0.091897, as well as $1^\circ 46' 22''$, $0^\circ 9' 17''$, and $0^\circ 35' 47''$ separately. Only one of the planets (m_2) survived after the close encounters. The orbital evolutions of the three planets are shown in Figure 1.

As shown in Figure 1, eccentricities of all the planets are excited to large values during the scattering, while inclinations of m_2 and m_3 remain low. The spin axes of m_1 and m_2 are both tilted. In particular m_1 has large and fast spin inclination (θ) variations before it is ejected (phase 2, yellow region). This is because the inclination of m_1 is excited above 50° , and spin-axis precession around the orbit drives large amplitude spin-axis variations. In addition, the semimajor axis of m_1 becomes small before the ejection, and this leads to fast spin-precession rate and thus fast oscillations in θ .

On the other hand, m_2 ’s obliquity (ϵ) is slightly increased during phase 1 (green region) due to orbital inclination increase. Then, its spin inclination (θ) is largely tilted during the second close encounter of the planets (phase 3, red region around ~ 0.1 – ~ 0.2 Myr), while the orbital inclination remains low. After the ejection of m_3 , the obliquity of m_2 remains constant, and the spin-axis inclination variations are caused by spin-axis precession around the orbital normal direction due to spin–orbit coupling.

How is the spin axis of m_2 tilted? To investigate the mechanisms that tilt the spin axis of the surviving planet m_2 , we plot the obliquity and spin evolution using both the N -rigid-body simulation and the secular approach. We note that it is not

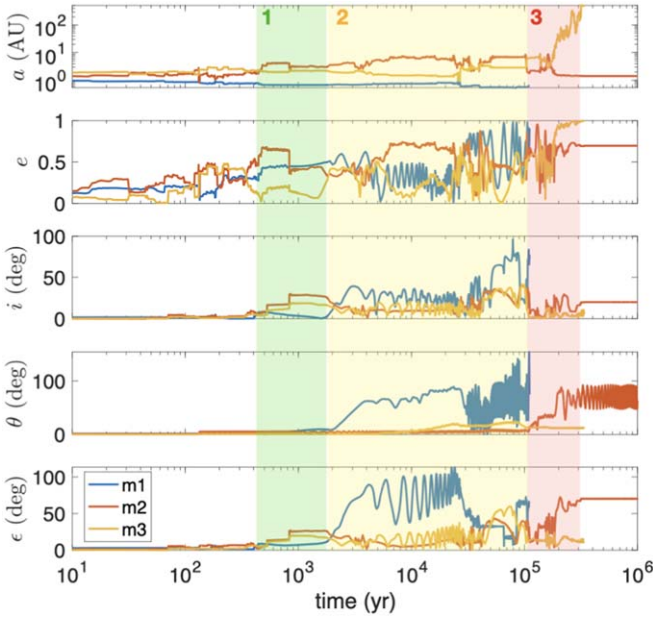


Figure 1. Illustrative example of a scattering experiment. θ and ϵ represent the tilt of the spin axis relative to the reference plane and the spin-orbit misalignment (obliquity) separately. Both planet m_1 and m_2 's spin axes are largely tilted during the scattering process, and planet m_2 's inclination remains low $\sim 20^\circ$ after the encounter.

appropriate to use the secular method to estimate the evolution of the system during planet-planet scattering, where the semimajor axes change drastically. However, we use it as a probe to illustrate the effects of the nonadiabatic resonance between the spin and orbital precessions that enhanced spin inclinations. This is analogous to the secular spin-orbit resonance encounters during planet migration (e.g., Vokrouhlický & Nesvorný 2015; Millholland & Laughlin 2019), while the semimajor axes changes can be more drastic during scattering. We plot the precession rate of the spin axis and that of the orbital longitude of ascending node in Figure 2. The secular results are obtained following the Hamiltonian listed below (e.g., Laskar & Robutel 1993):

$$H(\xi, \psi, t) = \frac{1}{\alpha} \xi^2 + \sqrt{1 - \xi^2} (A(t) \sin \psi + B(t) \cos \psi), \quad (3)$$

where $\xi = \cos \epsilon$, ψ is the spin longitude projected in the orbital plane, and α is the spin-precession coefficient (e.g., Ward & Hamilton 2004):

$$\begin{aligned} \alpha &= \frac{k_2}{2C} n \left[\frac{\omega R_p^3}{\omega_b a^3 (1 - e^2)^3} \right]^{1/2}, \\ &= 5.9 \times 10^{-4} \text{ yr}^{-1} \\ &\times \left(\frac{k_2/(2C)}{0.5/0.52} \right) \left(\frac{n}{2\pi \text{ yr}^{-1}} \right) \left[\frac{\omega/\omega_b}{0.3} \frac{(R_p/R_{\text{jup}})^3}{(a/1 \text{ au})^3 (1 - e^2)^3} \right]^{1/2} \end{aligned} \quad (4)$$

where n is the orbital frequency, and ω and ω_b are the spin velocity and the breakup velocity of the planet. In addition, $A(t)$ and $B(t)$ reflect the orbital variations and are expressed as

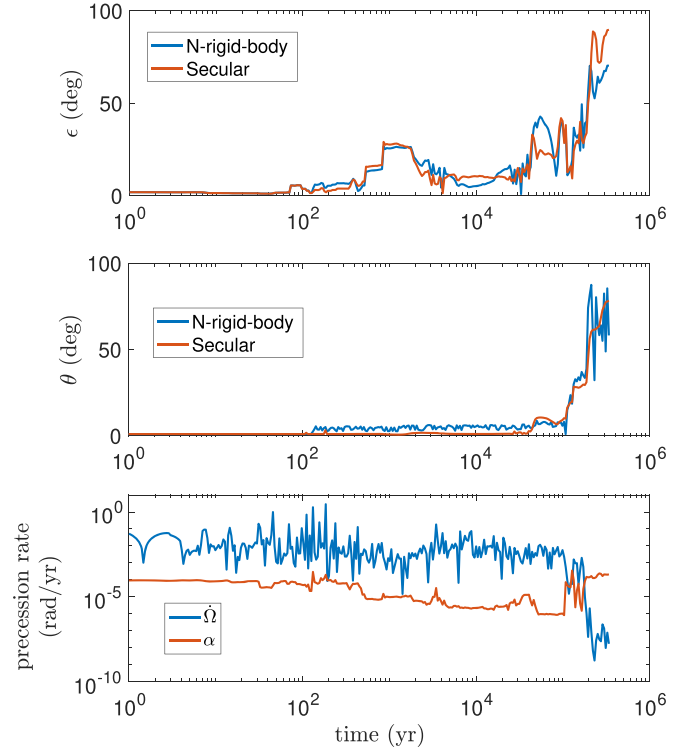


Figure 2. Obliquity and spin evolution (top two panels) compared with the spin and orbital precession rate (bottom panel). In the top two panels, the blue lines represent the results of the N -rigid-body simulation, and the red lines represent the secular results. The secular results largely agree with the N -rigid-body simulations, and disagreement is expected since secular approximation is not valid during planetary close encounter when the orbital elements have rapid changes. The bottom panels show the precession rates. It illustrates that when the spin-precession rate coincides with that of the orbital precession, the spin axis of the planet is tilted.

follows:

$$A(t) = 2(\dot{q} + p(q\dot{p} - p\dot{q})) / \sqrt{1 - p^2 - q^2} \quad (5)$$

$$B(t) = 2(\dot{p} - q(q\dot{p} - p\dot{q})) / \sqrt{1 - p^2 - q^2}, \quad (6)$$

where $p = \sin i/2 \sin \Omega$ and $q = \sin i/2 \cos \Omega$. We obtain the orbital evolution using the results of the N -rigid-body simulations and integrate the spin evolution using the secular approach before the ejection of m_3 .

For the precession rates, the orbital precession time is directly obtained taking the time derivative of the longitude of the ascending node (Ω), and we use the spin-axis precession coefficient α as a proxy for the spin-axis precession rate.

As shown in Figure 2, obliquity of the planet is increased during the first close encounter between the planets around ~ 1 kyr. The inclination of m_2 is excited, while the spin-axis inclination (θ) is not affected significantly during the close encounter. Thus, obliquity is increased due to changes in the orbital inclination. Next, at ~ 0.1 Myr, after the close encounter between m_2 and m_3 , the semimajor axis of m_2 is reduced, which leads to faster spin-precession rate. Meanwhile, the orbital precession rate decreases as the planet companion m_3 scatters with m_2 and migrates outward. This causes sweeping of spin-orbit resonance, which drives obliquity excitation and the tilt of the spin axis while the inclination of the orbit remains low ($\sim 20^\circ$).

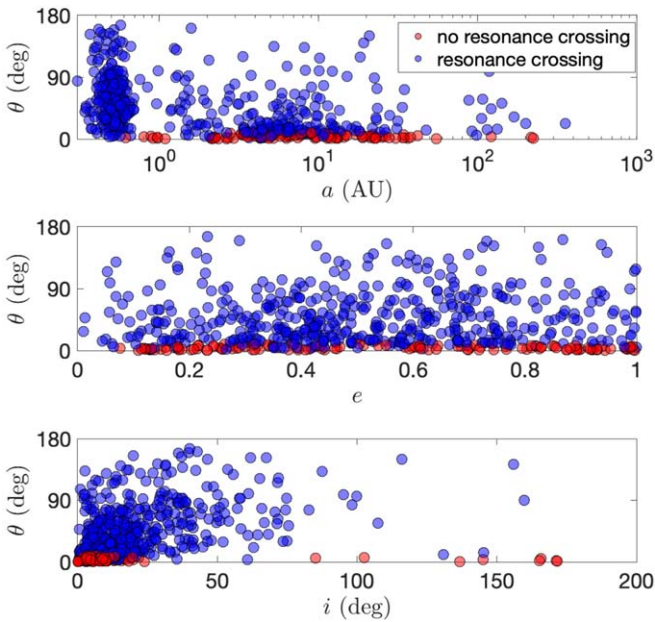


Figure 3. Results of scattering experiments. Tilt of planetary spin axis as a function of planet semimajor axis (top panel), eccentricity (middle panel), and inclination (bottom panel). Red circles mark the runs that did not encounter spin–orbit resonance crossing, and blue circles mark those that did encounter the resonance crossing. Eccentricity and inclination can be excited to large values during planet scattering, and there is a wide spread in eccentricity and inclination for large tilt of planetary spin axis. It is easier for planetary spin axis to tilt with larger planet inclination, due to precession of the spin axis around the orbital normal.

2.3. Scattering Results

We run 500 scattering experiments to study the distribution in the tilt of the planetary spin axes during planet–planet scattering. We sample the orbital parameters and masses of the planets as described in Section 2.1. $\sim 60\%$ of the scatterings avoid planet–planet collisions. We focus on systems that have no collisions, and the results are summarized in this section.

Figure 3 shows the tilt of the spin axis with respect to semimajor axes, eccentricities, and inclinations of the planets. The dearth of planets around ~ 1 au is due to planet–planet scattering as the innermost planets start at 1 au. There is a wide spread in semimajor axes, eccentricities, and inclinations for planets with large spin-axis inclination (θ). The dependence of the spin-axis inclination on the final eccentricity of the planets is weak, but it is more likely to tilt the spin axis of the planets with larger final inclinations. This is because spin-axis precession around the orbit leads to larger spin-axis inclination when the orbit is more inclined relative to the reference plane. In addition, the obliquity oscillation amplitude is larger with higher inclination under spin–orbit resonances (e.g., Shan & Li 2018).

To investigate the role of spin–orbit resonances, we mark the runs that encountered the spin–orbit resonance crossing (with matching spin-precession frequency and orbital precession frequency) in blue. Spin-orbit resonances are prevalent during scattering. Specifically, 80.2% of the systems encountered spin–orbit resonances, and all systems with spin inclination excited above 10° encountered spin–orbit resonance crossing. Systems with lower semimajor axes have a larger probability to encounter spin–orbit resonances (97.8% for $a < 1$ au) compared to their farther companions (66.0% for $a > 1$ au). Some systems have spin inclination enhanced due to both orbit

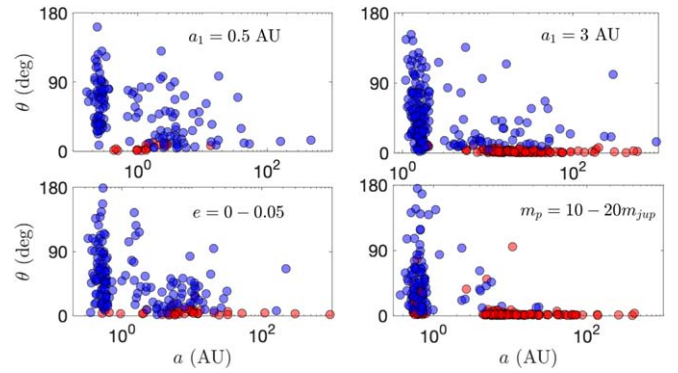


Figure 4. Tilt of planetary spin axis as a function of planet semimajor axis for different sets of scattering experiments. The setup of the simulations is the same as that described in Section 2.1, except that in the upper left panel the innermost planet starts at 0.5 au; in the upper right panel the innermost planet starts at 3 au; in the lower left panel the initial eccentricities range between 0 and 0.05; and in the lower right panel the planet masses range between 10 and $20m_{\text{jup}}$. Similar to Figure 3, red circles mark the runs that did not encounter spin–orbit resonance crossing, and blue circles mark those that did encounter the resonance crossing. It is easier for planetary spin axes to tilt for close-in planets in all the scattering experiments, and the planetary spin axes can be tilted to larger values for planets with higher v_{orb} to v_{esc} ratios.

precession and spin–orbit resonances. Overall, it is more likely to tilt the planetary spin axis with low semimajor axis due to faster spin-precession rates that are both more likely to commensurate with that of orbital precession, and to tilt the spin axis around orbital normal more efficiently.

Precession timescales are longer for farther companions (e.g., ~ 10 Myr at 10 au for a Jupiter-like planet), and this will enhance planetary spin inclination over long timescales when planetary spin axes precess around inclined orbits. We note that we only focus on the outcomes shortly (1 Myr) after planet–planet scattering, and the detailed long-term dynamics will be discussed in a follow-up study.

3. Parameter Studies

We consider different scattering experiments in this section, varying the distribution of the initial eccentricity, semimajor axes, and the mass of the planets. For each set of simulations, we run 200 experiments. The distributions of the spin-axis inclinations as a function of the planets’ final semimajor axes are shown in Figure 4.

The upper panels of Figure 4 include different initial semimajor axes of the innermost planets compared to the default set of simulations in Section 2.3. As the planets reside farther from the host star, the orbital velocity decays, and planets can avoid collisions more easily (with lower ratio of the orbital velocity to the escape velocity, see, e.g., Petrovich et al. 2014). However, the spin-axis inclination of the planets can be more easily excited, when the planets start closer to the host stars due to faster spin precession rates. Thus, fewer planets have their spin axes tilted during scattering when starting farther from the host star, even though more of them avoid collisions.

The lower left panel shows the case in which the planets start less eccentric (e ranging between 0 and 0.05). It takes more time for the eccentricity to grow larger due to planet interactions, and orbital instability occurs at a later time. Nevertheless, spin-axis inclination distribution and its dependence on semimajor axis are similar comparing to the default set

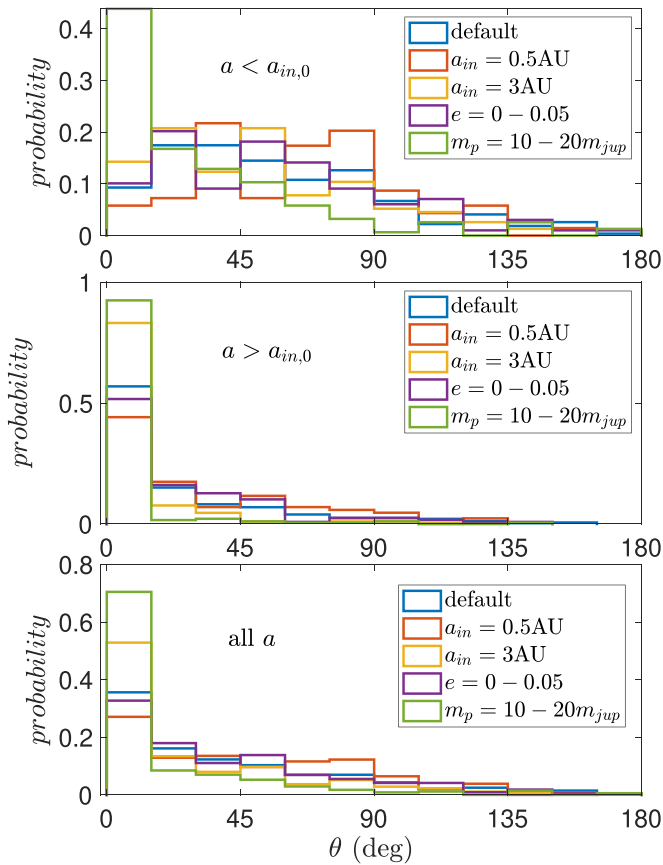


Figure 5. Histogram of the spin-axis inclination for planets with final semimajor axes interior (upper panel) and exterior (lower panel) to the initial semimajor axes of the innermost planets. Planets with higher $v_{\text{orb}}/v_{\text{esc}}$ ratios residing closer to the host star can more easily tilt their spin axes.

of simulations in Section 3. Note that the distribution of the spin-axis inclination is shown more clearly in Figure 5.

When the masses of the planets get larger, the escape velocities increase, and planets experience faster ejection. Thus, as shown in the lower right panel of Figure 4 with planet masses ranging between $10m_{\text{jup}}$ and $20m_{\text{jup}}$, fewer planets have their spin axes tilted to large values.

Similar to Figure 3, we mark the runs that encountered spin-orbit resonance crossing in blue. It is more likely to encounter spin-orbit resonances when the planet starts closer to the host star due to the faster precession rates (89.0% starting at 0.3 au versus 59.6% starting at 5 au). Larger planetary masses ($10m_{\text{jup}}$ and $20m_{\text{jup}}$) are less likely to encounter spin-orbit resonances due to faster ejection processes (37.9%), and lower initial eccentricities ($e = 0-0.05$) do not change the probability of encountering the spin-orbit resonances significantly (79.2%). As expected, spin inclinations are more likely to be enhanced for systems that encounter spin-orbit resonance crossing.

For all the sets of simulations, planets with lower final semimajor axes can have their spin axes tilted more easily immediately (1 Myr) after the scattering. This is both due to the higher probability to cross spin-orbit resonances closer to the host star and due to the stronger nonadiabatic limit farther from the host star that cannot efficiently excite spin inclination. Thus, in Figure 5 we divide the sample into two groups: those with final semimajor axes lower than the initial semimajor axes of the innermost planets (upper panel), and those that reside farther (middle panel).

Most close-in planets could have large spin-axis inclination, except those with large masses (or low $v_{\text{orb}}/v_{\text{esc}}$ ratio). Those that initially reside closer to the host star can have spin axes excited to larger values. The differences in the initial eccentricities do not have a significant influence on the distribution of the final spin-axis inclinations.

The majority of planets with large separation from their host star still have low spin-axis inclination even though some planets could have their spin-axis inclination excited. Comparing different initial conditions of the scatter experiments, the difference in the initial eccentricity also has little effect on the final distribution of the spin-axis inclination. When the planetary masses are higher or start farther from the host star (lower $v_{\text{orb}}/v_{\text{esc}}$ ratio), it is more difficult to excite the planetary spin axes due to faster planet ejection processes.

Combining the two groups together (bottom panel), $\sim 50\%$ of the scattering experiments produce high spin-axis inclinations over 50° when the planets start at 0.5 au, and $\sim 20\%$ – 30% produces high spin-axis inclinations starting at 1–3 au. Only around $\sim 10\%$ reach high spin-axis inclination for massive planets ($10-20m_{\text{jup}}$).

After the completion of this paper, we became aware of a complementary study that arrived at the same results independently and simultaneously based on two-planet scattering (Hong et al. 2021). Our results about the dependence of planetary spin-axis inclination on semimajor axes agree with each other. In addition, our results show that three-planet scatterings could lead to a larger number of planets with higher obliquity due to longer instability time and higher inclination excitation.

4. Conclusion and Discussion

In this Letter, we discuss planetary spin-axis variations during planet scattering. We find that temporary spin-orbit resonances could lead to large tilt of planetary spin axes for planets with a wide range of eccentricities and inclinations. It is more likely for planetary spin axes to tilt for planets that have lower masses and initially reside closer to the host star before scattering occurs (higher $v_{\text{orb}}/v_{\text{esc}}$ ratio), which could allow for slower ejection processes and longer time to tilt the planets. In addition, it is more likely to tilt the spin axes of the planets that reside closer to the host stars after planet-planet scattering.

We note that the spin-axis inclination of the massive planet in system 2M0122 is unlikely due to spin-orbit resonances during planet scattering. Orbiting around a $0.4M_{\odot}$ star, the escape velocity of the $12-27m_{\text{jup}}$ planet greatly exceeds the orbital velocity. The ejection process is fast and could quench obliquity excitation due to secular resonances. Thus, it is challenging to produce planets with large obliquities, particularly at distances around ~ 50 au. It is likely that the tilt of the planet is due to turbulent accretion or the tilt of the circumplanetary disk (Bryan et al. 2020; Martin et al. 2020). In addition, as a caveat, recent SPH simulations have shown that collision rate could be further increased, and this will lower the probability of planetary spin-axis tilt during planet-planet scattering (Li et al. 2021).

Many mechanisms have been proposed to explain the origin of tilted planetary spin axes. For instance, planet-disk interactions, turbulent accretion to planets, and collisions during planet-planet scattering can also lead to misaligned planetary spin axes. To distinguish from the other scenarios, planet-planet scattering (with no collisions) could lead to

planets with a wide range of eccentricities and inclinations. In addition, planetary spin rate is nearly unchanged, differing from those produced by planet collisions. Obliquity presents an exciting and unique window into formation history, and more systems with measured obliquities will enable statistical studies to disentangle different planet formation mechanisms in the future.

The author thanks Fred Adams, Smadar Naoz, Konstantin Batygin, Zeev Rogozzinski, and Dong Lai for reading the manuscript and providing helpful comments. The author also thanks the referee for helpful comments, which greatly improved the quality of the Letter. G.L. is grateful for the partial support by NASA 80NSSC20K0641 and 80NSSC20K0522.

ORCID iDs

Gongjie Li  <https://orcid.org/0000-0001-8308-0808>

References

- Adams, F. C., & Laughlin, G. 2003, *Icar*, **163**, 290
 Anderson, K. R., Lai, D., & Pu, B. 2020, *MNRAS*, **491**, 1369
 Barnes, J. W., & Fortney, J. J. 2003, *ApJ*, **588**, 545
 Bryan, M. L., Chiang, E., Bowler, B., et al. 2020, *AJ*, **159**, 181
 Carter, J. A., & Winn, J. N. 2010, *ApJ*, **716**, 850
 Chambers, J. E., Wetherill, G. W., & Boss, A. P. 1996, *Icar*, **119**, 261
 Chatterjee, S., Ford, E. B., Matsumura, S., & Rasio, F. A. 2008, *ApJ*, **686**, 580
 Chen, R., Li, G., & Tao, M. 2021, arXiv:2103.12767
 Ford, E. B., & Rasio, F. A. 2008, *ApJ*, **686**, 621
 Freikh, R., Jang, H., Murray-Clay, R. A., & Petrovich, C. 2019, *ApJL*, **884**, L47
 Gaidos, E., & Williams, D. M. 2004, *NewA*, **10**, 67
 Goldreich, P., Lithwick, Y., & Sari, R. 2004, *ApJ*, **614**, 497
 Hong, Y.-C., Lai, D., Lunine, J. I., & Nicholson, P. D. 2021, arXiv:2103.15902
 Ida, S., & Lin, D. N. C. 2004, *ApJ*, **604**, 388
 Kane, S. R., & Torres, S. M. 2017, *AJ*, **154**, 204
 Kokubo, E., & Ida, S. 2002, *ApJ*, **581**, 666
 Laskar, J., & Robutel, P. 1993, *Natur*, **361**, 608
 Lee, M. H., Peale, S. J., Pfahl, E., & Ward, W. R. 2007, *Icar*, **190**, 103
 Li, G., & Batygin, K. 2014, *ApJ*, **790**, 69
 Li, J., & Lai, D. 2020, *ApJL*, **898**, L20
 Li, J., Lai, D., Anderson, K. R., & Pu, B. 2021, *MNRAS*, **501**, 1621
 Lin, D. N. C., & Ida, S. 1997, *ApJ*, **477**, 781
 Lissauer, J. J. 1993, *ARA&A*, **31**, 129
 Martin, R. G., Zhu, Z., & Armitage, P. J. 2020, *ApJL*, **898**, L26
 Millholland, S., & Batygin, K. 2019, *ApJ*, **876**, 119
 Millholland, S., & Laughlin, G. 2019, *NatAs*, **3**, 424
 Morbidelli, A., Tsiganis, K., Batygin, K., Crida, A., & Gomes, R. 2012, *Icar*, **219**, 737
 Murray, C. D., & Dermott, S. F. 2000, *Solar System Dynamics* (Cambridge: Cambridge Univ. Press)
 Mustill, A. J., Davies, M. B., & Johansen, A. 2017, *MNRAS*, **468**, 3000
 Petrovich, C., Tremaine, S., & Rafikov, R. 2014, *ApJ*, **786**, 101
 Quarles, B., Barnes, J. W., Lissauer, J. J., & Chambers, J. 2020, *AsBio*, **20**, 73
 Quarles, B., Li, G., & Lissauer, J. J. 2019, *ApJ*, **886**, 56
 Quillen, A. C., Chen, Y.-Y., Noyelles, B., & Loane, S. 2018, *CeMDA*, **130**, 11
 Rasio, F. A., & Ford, E. B. 1996, *Sci*, **274**, 954
 Rogozzinski, Z., & Hamilton, D. P. 2020, *ApJ*, **888**, 60
 Saillenfest, M., Lari, G., Boué, G., & Courtot, A. 2021, *A&A*, **647**, A92
 Saillenfest, M., Laskar, J., & Boué, G. 2019, *A&A*, **623**, A4
 Schwartz, J. C., Sekowski, C., Haggard, H. M., Pallé, E., & Cowan, N. B. 2016, *MNRAS*, **457**, 926
 Shan, Y., & Li, G. 2018, *AJ*, **155**, 237
 Slattery, W. L., Benz, W., & Cameron, A. G. W. 1992, *Icar*, **99**, 167
 Su, Y., & Lai, D. 2020, *ApJ*, **903**, 7
 Touma, J., & Wisdom, J. 1993, *Sci*, **259**, 1294
 Touma, J., & Wisdom, J. 1994, *AJ*, **107**, 1189
 Vokrouhlický, D., & Nesvorný, D. 2015, *ApJ*, **806**, 143
 Ward, W. R. 1973, *Sci*, **181**, 260
 Ward, W. R., & Hamilton, D. P. 2004, *AJ*, **128**, 2501